Journal of Fluids and Structures (2001) **15,** 909–928
doi:10.1006/jfls.2001.0384, available online at http://www.idealibrary.com on IDEAL®

HYDRODYNAMIC DAMPING AND QUASI-COHERENT STRUCTURES AT LARGE STOKES NUMBERS

T. SARPKAYA

Mechanical Engineering, Naval Postgraduate School, Monterey, CA 93943, U.S.A.

(Received 4 December 2000, and in final form 14 February 2001)

Unsteady flow about solid and perforated cylinders at large Stokes numbers and very small Keulegan–Carpenter numbers has not been sufficiently understood to predict the hydroelastic response of compliant structures subjected to high frequency excitation. It is impossible to compute, difficult to quantify, and extremely difficult to visualize. Here, following a brief review of the previous research, new results for both forced and pluck-induced oscillations are presented. It is shown that: (a) the measured drag coefficients are larger (about double for smooth cylinders) than those predicted from the Stokes–Wang analysis (in the region of its applicability); (b) there is an unstable flow regime in which the oscillatory boundary layer develops quasicoherent structures (QCS) over a range of K values before giving rise to Honji-type coherent structures (HTCS); (c) the drag coefficients for perforated cylinders are much larger than those for solid cylinders and do not follow the Stokes–Wang prediction even at small β. As expected, their inertia coefficients are considerably smaller than those for solid cylinders.

1. INTRODUCTION

HYDRODYNAMIC DAMPING is of considerable importance for structures undergoing dynamic excitation in the range of parameter space defined by very small Keulegan–Carpenter numbers ($K = 2\pi A/D$) and very large Stokes numbers ($\beta = Re/K = fD^2/\nu$), where $Re = U_{max}D/\nu$, D is the diameter of the cylinder, and A and U_{max} are the amplitudes of the displacement and velocity of the sinusoidal oscillations of frequency f, in a viscous fluid of kinematic viscosity ν. The reason for this is that typical K values for the Tension Leg Platforms are in the range of 0·005–0·02 and the large values of β mean large rates of vorticity diffusion, dictated by the prevailing instabilities (QCS and HTCS) to be discussed later.

Stokes' (1851) classical solutions formed the basis of many empirical and numerical models where the oscillations are presumed to be small enough to allow convective accelerations to be ignored. Stokes' solution for a circular cylinder, later extended to higher terms by Wang (1968), may be decomposed into in-phase and out-of-phase components as

$$C_a = 1 + 4(\pi\beta)^{-1/2} + (\pi\beta)^{-3/2}, \tag{1a}$$

$$C_d = \frac{3\pi^3}{2K}\left[(\pi\beta)^{-1/2} + (\pi\beta)^{-1} - \frac{1}{4}(\pi\beta)^{-3/2}\right], \tag{1b}$$

which shows the dependence of C_d and C_a on β and the fact that

$$\frac{C_a - 1}{KC_d} = \frac{8}{3\pi^3}, \tag{2}$$

0889–9746/01/070909 + 20 $35.00/0

in the limit as $K \to 0$ and $\beta \to \infty$. For example, for $KC_d = 0{\cdot}04$ one has $C_a = 1{\cdot}00344$. However, for $C_a = 1{\cdot}000344$, C_d is 10 times smaller than that for the same K with $KC_d = 0{\cdot}04$.

For sufficiently large values of β, equation (1b) may be approximated to

$$\{KC_d\sqrt{\beta}\}_{S-W} = 26{\cdot}24, \tag{3}$$

which shows that both $d(KC_d)/d\beta$ and KC_d approach zero asymptotically as β increases. However, the experiments reported herein show that KC_d approaches about 0·04 for the largest β values encountered.

The foregoing equations are valid only for sinusoidally oscillating, unseparated, stable, laminar flow about a smooth cylinder. Hall (1984) carried out a stability analysis of the unsteady *attached* boundary layer on a cylinder oscillating transversely in a viscous fluid in both linear and weakly nonlinear regimes. In order to simplify the problem, Hall further assumed that the oscillation frequency is large. This led to the critical Keulegan–Carpenter number given by

$$K_{cr} = 5{\cdot}78\beta^{-1/4}(1 + 0{\cdot}21\beta^{-1/4} + \cdots). \tag{4}$$

Equation (4) was entirely consistent with the experiments of Honji (1981) within the range of comparison ($70 < \beta < 700$). The fairly regular, mushroom-shaped instabilities observed by Honji, in a small range of β values, were previously named the "Honji instability" (Sarpkaya, 1986). They will now be renamed more precisely as the "Honji-type coherent structures, HTCS" in preparation for the discussion of irregular or "quasicoherent structure, QCS" occurring in oscillating boundary layers over a large but finite region of K values smaller than K_{cr}. The structures in the region $K > K_{cr}$ will be discussed later. It remains to be seen whether the QCS are responsible for the deviation of the measured drag coefficients from the Stokes–Wang prediction.

2. PREVIOUS INVESTIGATIONS

Considerable experimental work has been carried out in recent years on the hydrodynamic damping of circular cylinders in oscillatory flow: Sarpkaya (1986), in the range of $1035 < \beta < 11\,240$; Otter (1990) for $\beta = 61\,400$; Troesch & Kim (1991), for $\beta = 23\,200$ and 48 600; Bearman & Mackwood (1992), in the range $14\,371 < \beta < 30\,163$; Bearman & Russell (1996), for $\beta = 60\,000$; Chaplin & Subbiah (1998), for $\beta < 166\,900$; Chaplin (2000), for $\beta = 670\,000$ and 1 277 000; and Sarpkaya (2000), for $\beta = 748\,000$ and 1 365 000 for smooth, sand-roughened ($k/D = 1/100$) and porous (30% porosity) pipes. These are shown in Tables 1(a)–1(c) together with some of the more important characteristics of the experiments. In these tables, the published $KC_d\beta^{1/2}$ values are discussed through the use of a parameter Λ_K defined as

$$\Lambda_K = [\{KC_d\sqrt{\beta}\}_{Exp}/\{KC_d\sqrt{\beta}\}_{S-W}]_K, \tag{5}$$

where $(KC_d\beta^{1/2})_{S-W} \approx 26{\cdot}24$ is the classical laminar flow solution of Stokes and Wang. It should be noted that Λ_K is meaningful only at very small K values. Every attempt has been made to choose the smallest K at each investigation. The data for small K may be represented either by multiplying the constant 26·24 by Λ_K or by multiplying ν in β by $(\Lambda_K)^2$. In the latter case, $(\Lambda_K)^2$ transforms the kinematic viscosity to a virtual or eddy kinematic viscosity (*à la* Boussinesq). The relative roughness of the surface of the cylinder is given by k/D. Other parameters of interest, not shown in these abridged tables, are

$$KC_d = 26{\cdot}24\beta^{-1/2}, \tag{6}$$

TABLE 1(a)
Values of the various experimental parameters for the data obtained by the references noted (1986–1991)

References	Λ	$v_t/v = \Lambda^2$	β fD^2/v	K_{cr}	k/D	Exper. system
Sarpkaya (1986)	Before Honji inst. $\Lambda_{0\cdot4} = 1$	1	1035	(0·62) 1·057	Smooth	U-tunnel
Sarpkaya (1986)	After Honji inst. $\Lambda_{0\cdot4} = 1\cdot4$	1·96	1035	(0·62) 1·057	Smooth	U-tunnel
Sarpkaya (1986)	$\Lambda_{0\cdot5} = 3\cdot7$	13·7	1800	0·916	1/100	U-tunnel
Sarpkaya (1986)	$\Lambda = ?$ K_{min} not small enough		11 240	0·56	Smooth	U-tunnel
Otter (1990)	1 for $K < K_{cr}$	1	61 400	0·39	Smooth	E-M shaker
Troesch & Kim (1991)	$\Lambda_{0\cdot1} = 2$ Before Honji inst.	4	23 200	0·47	Smooth	Forced vib. at resonance
Troesch & Kim (1991)	$\Lambda_{0\cdot1} = 3\cdot75$ After Honji inst.	14	23 200	0·47	Smooth	Forced vib. at resonance
Troesch & Kim (1991)	$\Lambda_{0\cdot1} = 4\cdot45$	19·8	48 000	0·39	Smooth	Forced vib. at resonance

TABLE 1(b)
Values of the various experimental parameters for the data obtained by the references noted (1992)

References	Λ	$v_t/v = \Lambda^2$	β fD^2/v	K_{cr}	k/D	Exper. system
Bearman & Mackwood (1992)	$\Lambda_{0\cdot1}$ 1·23–1·26	1·56	14 371–29 014	0·53–0·48	Smooth	Plucked pendulum
Bearman & Mackwood (1992)	$\Lambda_{0\cdot1}$ 1·80–2·20	3·24–4 ·84	13 800 21 000	0·53–0·50	1/100 1/50	Plucked pendulum
Bearman & Mackwood (1992)	$\Lambda_{0\cdot1} = 1\cdot8$	3·24	14 093	0·53	1/50	Plucked pendulum
Bearman & Mackwood (1992)	$\Lambda_{0\cdot1} = 2\cdot65$	7·0	27 313	0·45	1/100	Plucked pendulum
Bearman & Mackwood (1992)	$\Lambda_{0\cdot1} = 3\cdot18$	10·0	30 163	0·44	1/50	Plucked pendulum

the relative thickness of the Stokes layer,

$$\frac{\delta_{St}}{D} = 2\cdot82\beta^{-1/2}, \tag{7}$$

the oscillatory Reynolds number Re_δ defined by

$$Re_\delta = U_{max}\frac{\delta_{St}}{\nu} = 2\cdot82Re\,\beta^{-1/2}, \tag{8}$$

and the customary Reynolds number $Re = U_{max}D/\nu$, defined earlier.

TABLE 1(c)
Values of the various experimental parameters for the data obtained by the references noted (1996–2000)

References	Λ	$v_t/v = \Lambda^2$	β fD^2/v	K_{cr}	k/D	Exper. system
Bearman & Russell (1996)	$\Lambda_{0\cdot1} = 1\cdot45$	2·1	16 538	0·51	Smooth	Plucked pendulum
Bearman & Russell (1996)	$\Lambda_{0\cdot1} = 1\cdot92$	3·7	20 526	0·48	Smooth	Plucked pendulum
Bearman & Russell (1996)	$\Lambda_{0\cdot1} = 2\cdot0$	4	34 946	0·42	Smooth	Plucked pendulum
Bearman & Russell (1996)	$\Lambda_{0\cdot1} = 1\cdot87$	3·7	61 022	0·37	Smooth	Plucked pendulum
Chaplin & Subbiah (1998)	$\Lambda_{0\cdot1} = 2\cdot2$	4·8	166 900	0·29	Smooth	Forced vib. at resonance
Chaplin & Subbiah (1998)	$\Lambda_{0\cdot01} = 3$	9	166 900	0·29	1/1266	Forced vib. at resonance
Chaplin (2000)	$\Lambda_{0\cdot001} = 2$	4		0·20	Smooth	Free decay tests
	$\Lambda_{0\cdot001} = 2\cdot04$	4·16	670 000 1 277 000	0·17	Smooth	
Sarpkaya (2000)	For both β $\Lambda_{0\cdot002} = 2\cdot2$-for PL 2·4-for FV	For both β 4·84 5·76	748 000 1 365 000	0·197 0·169	Both smooth	Pluck and forced vib.
Sarpkaya (2000)	For both β $\Lambda_{0\cdot002} = 2\cdot2$-for PL 2·4 for FV	For both β 4·84 5·76	748 000 1 365 000	? ?	Both rough 1/100	Pluck and forced vib.

The results summarized in Tables 1(a)–1(c) have shown that drag coefficients are indeed inversely proportional to K in the region of no vortex shedding, but the Λ_K values exceed unity by varying amounts, except those of Sarpkaya (1986) for $\beta = 1035$ and 1380 and Otter (1990) for $\beta = 61\,400$. The most recent free-decay tests of Chaplin (2000) have shown that Λ_K remains at about 2 even for β values larger than 10^6. Sarpkaya's (2000) data, first reported at the IUTAM meeting in Marseille, yielded Λ_K values somewhat larger than 2. These will be discussed here in more detail later.

Some of the differences between the data summarized in Tables 1(a)–(c) may be attributed to the methods of experimentation, the use of pluck or forced oscillations, the range of β, methods of correction of the measured damping due to the structural and hydrodynamic damping of the supporting elements, free-surface and wall-proximity effects, cylinder surface roughness and aspect ratio, presence of air bubbles, etc. However, the consistency of the near doubling of the Λ_K at relatively large β can neither be denied nor explained away in terms of errors in otherwise carefully conducted experiments. This required an extensive investigation of the structure of the near-wall flow.

3. EXPERIMENTS

The experiments were conducted in three different facilities: a U-shaped water tunnel where the flow oscillated about cylinders at a constant frequency, in a rectangular basin where the test cylinder was subjected to forced oscillations at desired frequencies, and in a large reservoir where the horizontally mounted test cylinders were suspended between two

(sufficiently large) end-plates of a vertical pendulum in a large reservoir. The system was so designed that either pluck tests (free decay) or resonant-forced-vibration tests can be performed at frequencies as large as 6·0 Hz (in water) in the range of K values from about 0·001 to 0·55. The data (displacements, accelerations, forces, and strains) were sampled at a rate of 2500 Hz. A comprehensive uncertainty analysis (95% confidence interval) has shown that the uncertainty for the drag coefficient was less than 4·8%.

The nominal size of the cylinders ranged from 10 to 50 cm. The largest cylinder had a length-to-diameter ratio of 2. The smaller cylinders had larger L/D ratios. The most recent experiments reported herein were performed with two sets of cylinders: 35·56 and 49·50 cm smooth nonperforated cylinders and a 49·50 cm perforated cylinder (porosity = 30%). The solid cylinders were subsequently sand-roughened ($k/D = 1/100$, where D is the bare cylinder diameter here and elsewhere in this paper).

All pluck and forced-vibration experiments were repeated 3 times in air and 3 times in water (with cylinder in place) for each and every amplitude of oscillation. Then the cylinder was removed, and, as is customary [see, e.g., Bearman & Mackwood (1992)], all in air and in water experiments were repeated after replacing the removed cylinder mass (and its added mass) with equivalent weights (thin circular plates) attached to the sides of the modified end-plates (for area equivalency). The massive static and dynamic data from the linear-variable displacement transducers, accelerometers, force transducers, and strain gages were sufficient to determine the system stiffness, added mass, and the net hydrodynamic damping (here the logarithmic decrement) δ, corrected for the hydrodynamic damping of the submerged parts of the pendulum and the structural damping (the latter was indeed very low). Then, the drag coefficient was deduced from the well-known expression (Sarpkaya, 1978)

$$C_d = 3\pi m\delta/(2\rho D^2 \mathrm{K}), \tag{9a}$$

where C_d is the drag coefficient, m is the effective mass of the cylinder, and δ is the logarithmic decrement ($\approx 2\pi\zeta$, where ζ is the damping factor). Other parameters appearing in equation (9a) have been defined previously. For large values of β, the combination of equations (2) and (9a) yields

$$\zeta = \frac{1}{2}(C_a - 1)\frac{M_d}{m}, \tag{9b}$$

or

$$\mathrm{K}C_d = \frac{3\pi^3}{4}\zeta\frac{m}{M_d}, \tag{9c}$$

where M_d is the displaced mass of the cylinder per unit length. Equations (9a), (9c), and (6) show, for example, for $\mathrm{K}C_d = 0{\cdot}040$ that $\zeta m/M_d$ should not have an error larger than $\pm 0{\cdot}000172$ (corresponding to a variation of about $\pm 86\,000$ in β) to remain accurate within 10%. This, together with the example given in connection with equation (2), shows the extreme difficulty of the determination of $\mathrm{K}C_d$ for small values of K and large values of β. The concerns expressed above are equally valid for the forced vibration experiments also.

4. PRESENTATION OF DATA

4.1. Solid Cylinders

Preliminary plots of the drag coefficients as a function of K for the two solid cylinders ($\beta = 748\,000$ and $1\,365\,000$) have shown that there is no measurable difference between

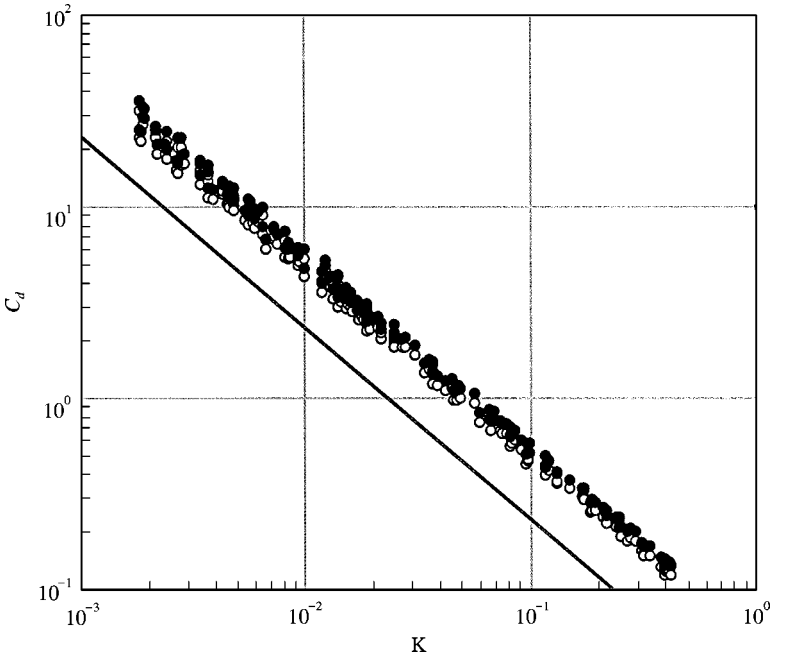

Figure 1. Drag coefficient versus Keulegan–Carpenter number for smooth solid cylinders at $\beta = 1\,365\,000$: ○, pluck tests; ●, forced oscillation; ——, theory (Stokes–Wang).

them. If anything, the difference is well within the scatter of the data. It is for this reason that the drag coefficients are presented herein only for $\beta = 1\,365\,000$.

Figures 1 and 2 show the drag coefficient C_d and the parameter Λ_K for pluck and forced-vibration experiments for $\beta = 1\,365\,000$. Several observations are rather obvious. There is some scatter in the data, the scatter decreasing with increasing K; the scatter is more apparent in Figure 2 and the mean lines through the data appear to have a small upward slope with increasing K. At $\beta = 1\,365\,000$ the drag coefficient, and hence Λ_K, is larger than that predicted by the Stokes–Wang (unseparated stable laminar flow) analysis in both the pre-Honji ($K_{cr} < 0{\cdot}169$) and post-Honji regimes, and that the forced-vibration tests yield somewhat larger C_d and Λ_K values. The average Λ_K values shown in Figure 2 are about 2·2 and 2·4 for the pluck and forced-vibration tests, respectively.

Figures 3 and 4 show C_d and Λ_K for the rough cylinder ($k/D = 1/100$) for $\beta = 1\,365\,000$. Their characteristics are similar to those shown in Figures 1 and 2 except that the effect of roughness increases Λ_K from 2·2 (for the smooth cylinder) to 3·2 for the rough cylinder. Forced vibration of the rough cylinders (not shown here) yielded an average Λ_K value of about 3·4, with equally large scatter. As will be amplified later, the scatter of the data is not entirely due to the shortcomings of the equipment and data evaluation. Some of the reasons are buried in the interstices of the roughness elements and the interaction between the roughness elements and the quasicoherent structures.

4.2. Perforated Cylinders

A perforated body is a rigid hollow shell whose surface is pierced by a distribution of small apertures which allow the near-free passage of fluid. The essential characteristics of flow through a perforated surface depend on the Reynolds number and Strouhal number based

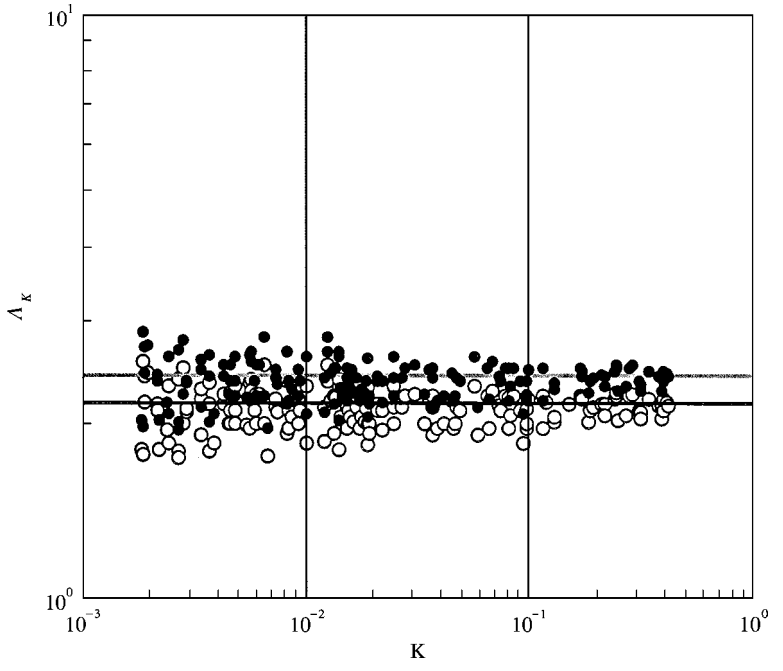

Figure 2. Λ_K versus Keulegan–Carpenter number for smooth solid cylinders at $\beta = 1\,365\,000$: ○, pluck tests; ●, forced oscillation; ——, theory (Stokes–Wang).

on the characteristic aperture diameter, on the relative spacing of the perforations, angle of the aperture to the incident flow, the ratio of the total open area to the total surface area of the body, whether or not the incident flow is laminar or turbulent, and on the Reynolds and Keulegan–Carpenter numbers of the cylindrical body.

The effect of flow unsteadiness in general and the added mass in particular has not been subjected to extensive theoretical, numerical, and experimental work. The existing works [e.g., Howe (1979), Molin (1992)] dealt with highly specialized cases and include the effect of perforations rather indirectly. The unsteady flow results show (Howe 1979) that perforations have a profound effect on the added mass and damping of the body. At very small amplitudes of oscillation or unidirectional surging, perforations reduce the added mass significantly since the body becomes transparent to the fluid motion. For porosities below about 30%, the added mass increases rapidly. Equally important is the fact that added mass also increases rapidly with increasing amplitude of oscillation for a given frequency and porosity.

Figure 5 shows the drag coefficient for the perforated cylinder (porosity = 30%, hole size = 1·168 mm, center-to-center spacing = 1·984 mm, and $\beta = 1\,365\,000$), together with that for the solid cylinder. The perforations considerably increase the drag (and hence the damping). The drag data were not expected to fall on a line parallel to the Stokes–Wang line for many reasons, the primary one being the fact that near the wall the flow is very complex and part of the flow goes through the cylinder and part around the cylinder. This is also the reason for the relatively small added-mass coefficient shown in Figure 6. The mean line through the perforated cylinder data in Figure 5 may be represented by $KC_d^{1\cdot3} = 0\cdot21$. The corresponding expression for the smooth solid cylinder is $KC_d = 0\cdot05$. It is evident that perforated cylinders, alone or in conjunction with a coaxial pipe or cable, can provide very large damping without increasing the added mass.

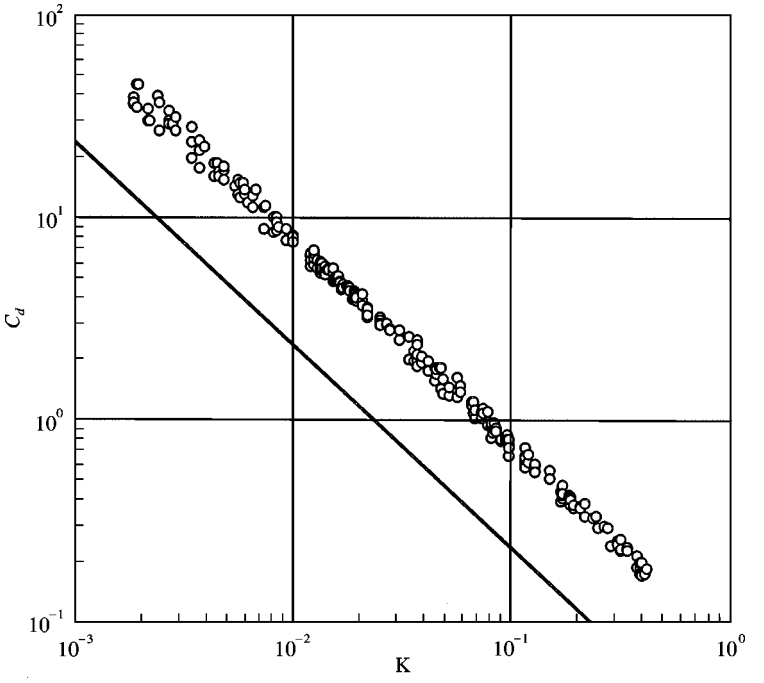

Figure 3. Drag coefficient versus Keulegan–Carpenter number for rough solid cylinders ($k/D = 1/100$) at $\beta = 1\,365\,000$: ○, pluck tests; ——, theory (Stokes–Wang).

4.3. Observations of Instabilities

The low-speed streaks and quasicoherent vortical structures are now considered to be ubiquitous features of a turbulent boundary layer near a solid wall, even though their origin still remains unresolved in both steady and periodic flows (Sarpkaya, 1993). Incisive as well as eloquent reviews of the state of the art, deduced from 40 years of experimentation and 10 years of numerical simulation of low-Reynolds-number canonical flows, have been given by Robinson & Kline (1990), Smith *et al.* (1991), and Robinson (1991). The studies on the instability of external oscillatory flows on curved walls are relatively new and dealt mostly with periodic sand ripples [see, e.g., Hara & Mei, (1990*a*,*b*), Scandura *et al.* (2000), and the references cited therein]. For understandable reasons, these studies dealt with relatively small Reynolds numbers and proved once again that the simulation of more realistic three-dimensional flows is beyond the present computing power. As noted earlier, Honji (1981) visualized the flow around a transversely oscillating cylinder in a fluid otherwise at rest and observed regularly spaced mushroom-shaped vortices along the two lines where the local ambient velocity is maximum. Subsequently, Sarpkaya (1986) named them "the Honji instability" and extended the range of observations to higher β values (about 5500). The use of direct numerical simulation at β values of interest here is not yet feasible. In fact, the only effort (to the best of our knowledge) to simulate the Honji instability was carried out by Zhang & Dalton (1999) at $\beta = 196$ using the primitive-variables form of the Navier–Stokes equations.

The present instability studies were conducted with forced oscillations of two cylinders ($D = 35{\cdot}56$ and $D = 49{\cdot}50$ cm, smooth and subsequently sand-roughened, $k/D = 1/100$). The reason for this is primarily the fact that the larger the cylinder the longer is the time (the

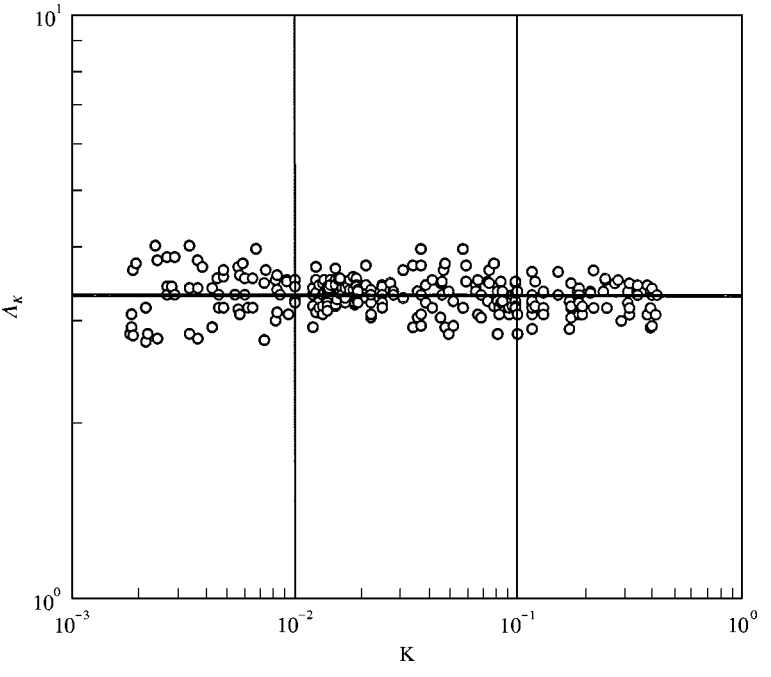

Figure 4. Λ_K versus Keulegan–Carpenter number for rough solid cylinders ($k/D = 1/100$) at $\beta = 1\,365\,000$: ○, pluck tests; ——, theory (Stokes–Wang).

number of cycles of oscillations) for the establishment of the Honji instability. Cylinders subjected to pluck tests did not always accord the opportunity for sufficiently long observations and recording. The rapidly decaying transient motions have transformed them into irregular vortical forms. This difference may partly account for the difference in the drag coefficients obtained from the pluck and forced-oscillation tests.

Flow visualization experiments were conducted using, with few minor exceptions, almost exactly the same instruments and procedures described in Sarpkaya (1986) and will not be repeated here. Water in the test tanks was circulated through a deaeration system prior to the experiments after it was discovered that the presence of small air bubbles and the attachment of some of them to the cylinder surface could interfere with or alter the character of the coherent or quasicoherent structures. The thickness of the dye layer, determined from the dye volume introduced and the area it spread on the cylinder was about 0·4 mm [25% of δ_{St}, given by equation (7)].

Each experiment began at a point defined by (β, K) in Figure 7. The thinner line, labeled H, after Hall (1984), represents equation (4). Each K on the Hall line corresponds to a critical K_{cr} at which the Honji instability occurs. The meaning of the cross-hatched line will emerge in the course of the following descriptions.

Experiments were carried out either by maintaining β constant (i.e., the frequency of oscillation) and decreasing K from an initial value of $K > K_{cr}$ down to K values smaller than K_{cr}, or by maintaining K constant and increasing β. Each change in either K or β is followed by a long rest and "refueling" (new dye introduction) period.

The cross-hatched line (marked S, denoting stability) in Figure 7 defines the approximate boundary that separates the stable region on the left from the unstable region on the right. It is the lower limit of the points defined by (β, K) where either no QCS are created

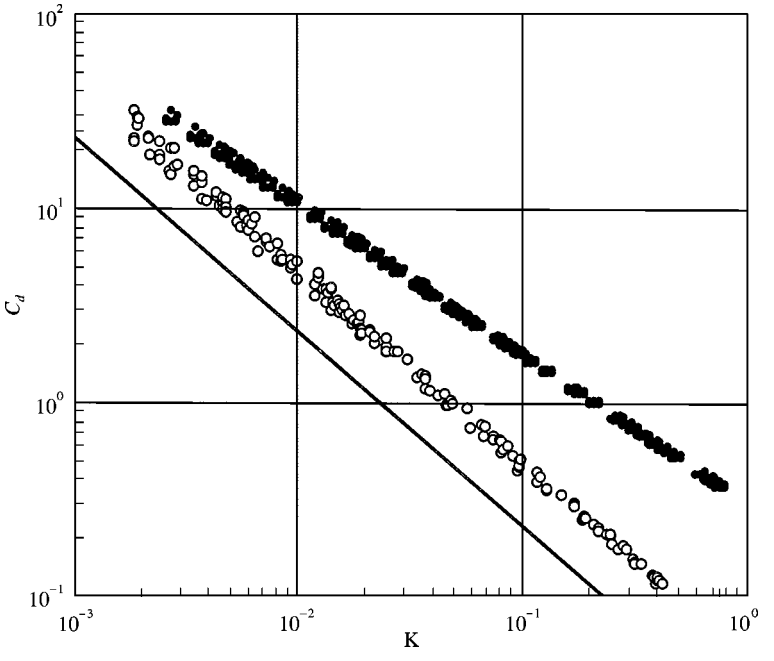

Figure 5. Drag coefficient versus Keulegan–Carpenter number: ○, pluck tests of smooth solid cylinders at $\beta = 1\,365\,000$ (see Figure 1); ●, pluck tests of the porous cylinder (30% porosity) at $\beta = 1\,365\,000$; ——, theory (Stokes–Wang).

during the entire cycle or those created (mostly during the high velocity period) barely survive the low velocity period. Part of the subjectivity, aside from human interpretation of the definition of the life of a QCS, comes from the fact that there cannot be a single line separating the stable region from the unstable region due to the statistical nature of the intermittency of the structures. In fact, the difficulty of the determination of the stability line cannot be adequately emphasized. It depends not only on the parameters that can be controlled but also on those which are, for all intents and purposes, beyond the capacity of the experimenter to control (e.g., temperature gradients, residual background turbulence, very small air bubbles, higher order harmonics of the vibrations, nonlinear interaction of various types of perturbations, etc.). Ironically enough, we are looking for the reasons as to why the flow does not become unstable at smaller K values in the region to the left of the line S.

A serious attempt was made to define a line K_l to the left of which no QCS are observed at any time during at least 20 cycles; to define another line, called K_f on which about half (as judged by eye) of the QCS (created during the high velocity period) survived the low velocity period (for about 20 cycles), and finally, to define a line K_g on which the QCS existed at all times, even though not at the same strength during both the low velocity and high velocity periods. This effort turned out to be extremely complex and not deterministic enough in view of the scatter in the data. It was eventually decided to reduce the boundary to a single line S (the average stability line) as defined above. The region between the lines S and H is where there always are QCS. The Hall line (or a very narrow region to the left and right of it) is where the well-known HTCS appear. In the region to the right of H one encounters, with increasing K, first HTCS, then QCS, and eventually, turbulence, separation and vortex shedding.

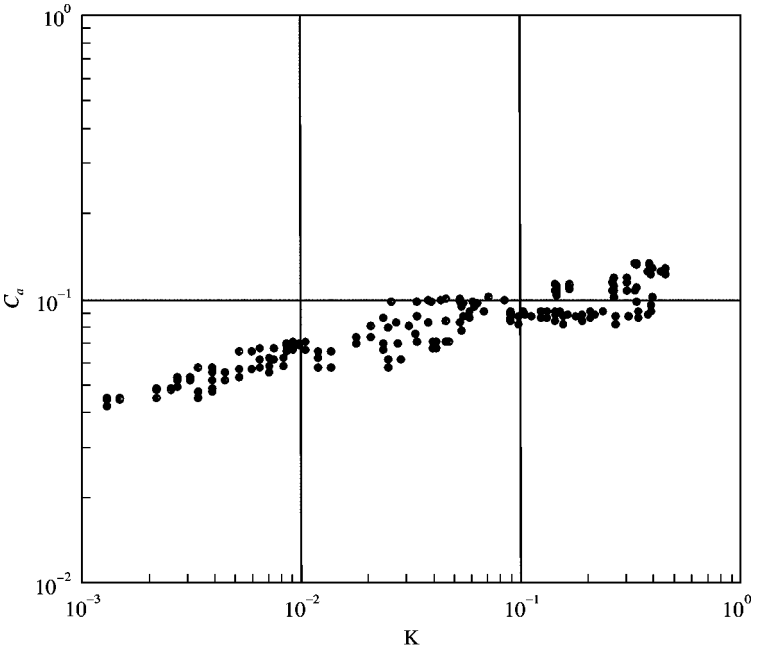

Figure 6. Inertia coefficient versus Keulegan-Carpenter number: ●, pluck tests of the porous cylinder (30% porosity) at $\beta = 1\,365\,000$.

Sufficient evidence exemplifying the various occurrences in each region in Figure 7 will now be presented. The descriptions to follow are based on extensive video viewing and the information extracted from it in terms of occurrence of various types of structures, mindful of the fact that the vagaries of flow visualization do not always provide correct insight into the physics of the actual occurrences. Furthermore, one can only repeat the complaint registered by practically all experimenters on this subject that still photographs (printed from the digitized frames of the video) do not convey as much information as motion pictures. Furthermore, it will be nearly impossible to provide photographic evidence of the events described for each and every data point. This will amount to reproducing about 650 000 frames that were used in following descriptions. It is also understood that no single realization at a given point in the β–K plane can ever exactly repeat itself. Thus, the figures should be regarded as examples of what might generally happen in the vicinity of a point in the β–K plane.

As far as the structures on the Hall line are concerned, Figure 8 corresponds to the point (1 365 000; 0·169). The characteristic features of the Honji instability (mushrooms) are apparent. The average relative spacing (s/D) between them (over 20 cycles of observations, beyond the initial period of establishment) is about 0·005. Some of the mushrooms occasionally rise above the others and then continuously evolve during the acceleration and deceleration periods even in a single cycle. Figure 9 shows another representative point (748 000; 0·197) on H. The average relative spacing between the mushrooms, again based on observations of more than 20 cycles, is about $s/D = 0{\cdot}0065$. Apparently, the instabilities at high β (Figures 8 and 9) are not as regular as those at much lower β values (e.g., Sarpkaya 1986). Figure 10 shows at (74 800; 0·35) representative mushrooms recorded during part of a single cycle (at 32 ms intervals) with an average $s/D = 0{\cdot}025$. Observations have shown that the structures, regardless of the number of cycles, do not necessarily acquire the same

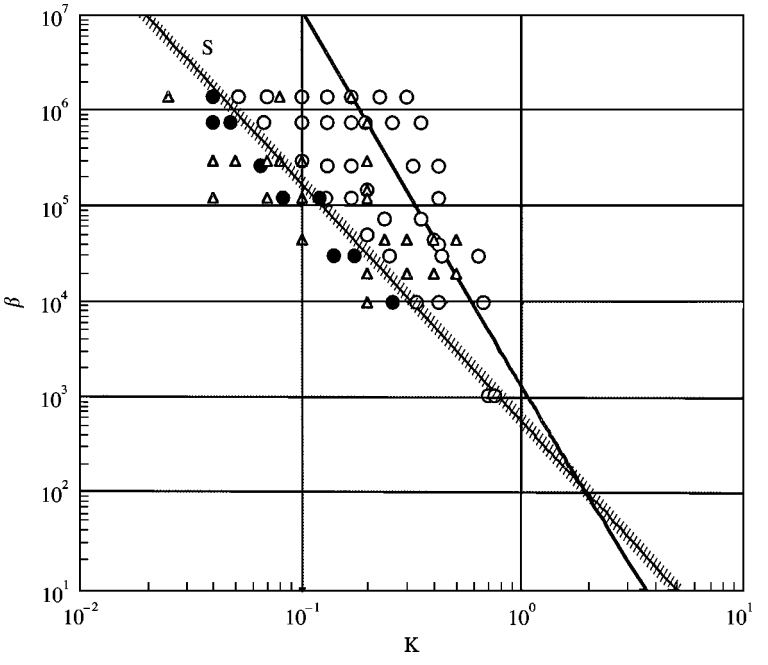

Figure 7. The β–K plane. Smooth cylinder: ●, stable region (no flow structures); ○, unstable region; ——, the Hall line (Honji instability); the cross-hatched line (only for the smooth cylinder) separates the stable region on the left from the unstable region on the right. Rough cylinder: △, quasicoherent structures at all points of observation.

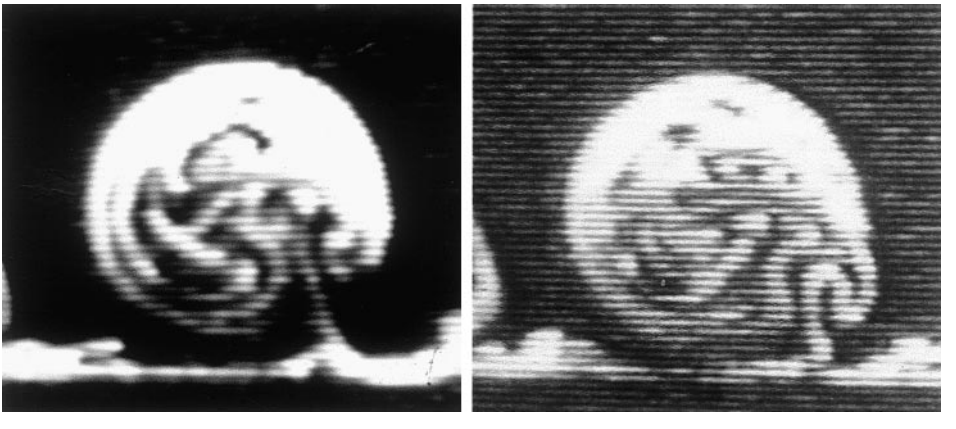

Figure 11. Enlarged views of two of the mushrooms shown in Figure 10. The occurrence of the Helmholtz instability is clearly visible.

size and shape at the same time. Some grow larger and others grow to the same size at a later time. Figure 11 shows the magnified versions of two of the mushrooms shown in Figure 10. It appears that the rollup of the vortex sheet is not smooth and Helmholtz instability may develop in mature mushrooms. The four representative strips from visualizations at (44 000; 0·4) on H are shown in Figure 12. They are relatively more regular with an average spacing of $s/D = 0{\cdot}034$.

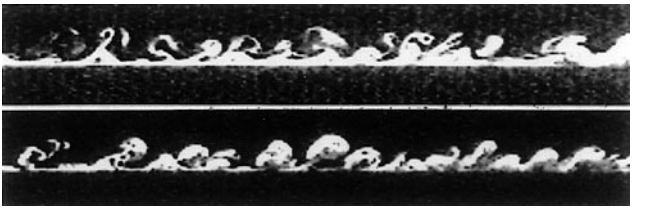

Figure 8. Representative Honji-type coherent structures at $\beta = 1\,365\,000$ and K = 0·169.

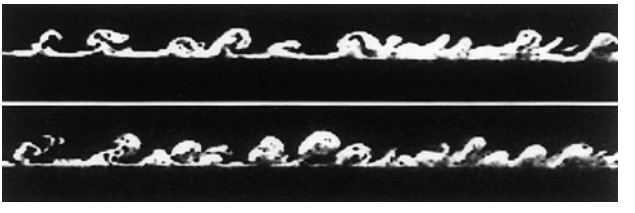

Figure 9. Representative Honji-type coherent structures at $\beta = 748\,000$ and K = 0·197.

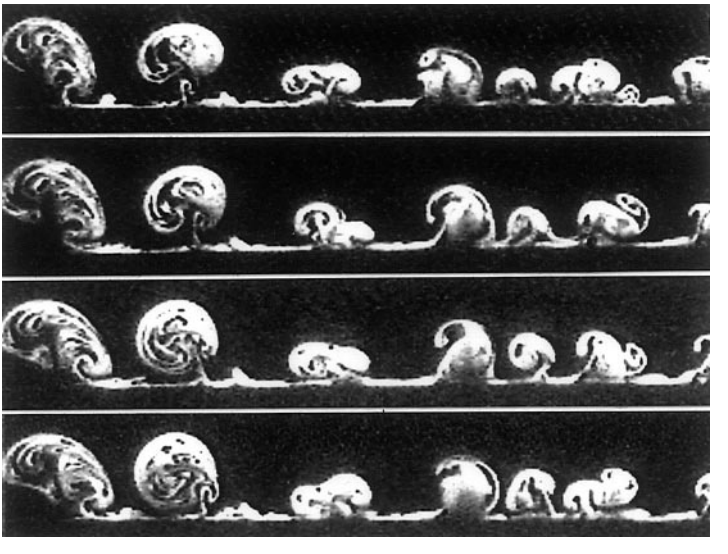

Figure 10. Representative Honji-type coherent structures at $\beta = 74\,800$ and K = 0·35.

doi:10.1006/jfls.2001.0384

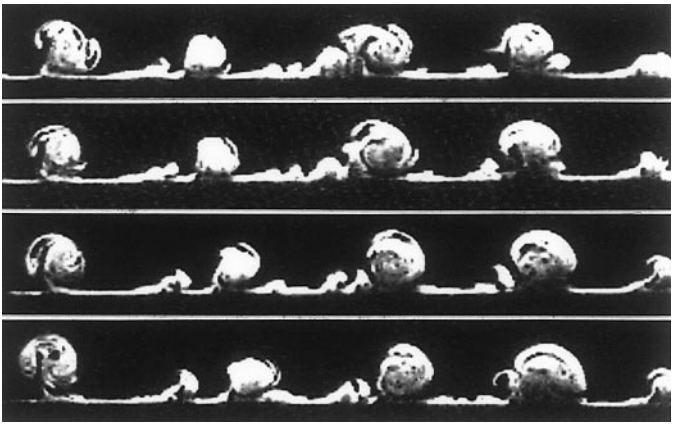

Figure 12. Representative Honji-type coherent structures at $\beta = 44\,000$ and $K = 0{\cdot}40$.

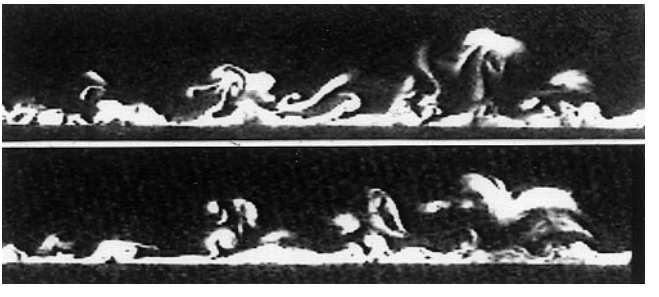

Figure 13. Representative quasicoherent structures at $\beta = 1\,365\,000$ and $K = 0{\cdot}30$ ($= 1{\cdot}8K_{cr}$).

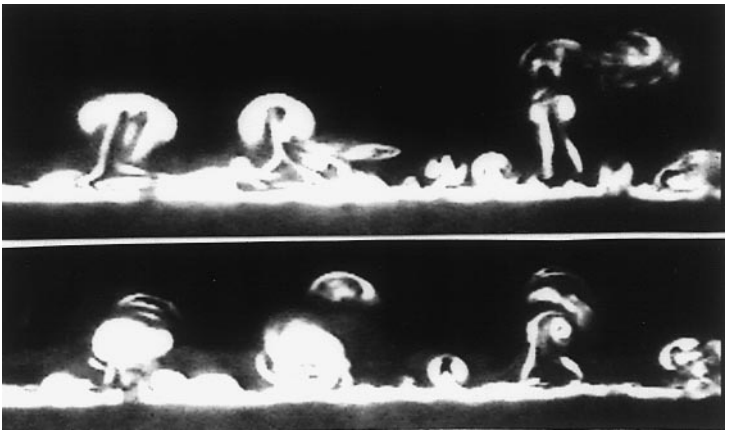

Figure 14. Representative quasicoherent structures at $\beta = 120\,000$ and $K = 0{\cdot}42$ ($= 1{\cdot}36K_{cr}$).

doi:10.1006/jfls.2001.0384

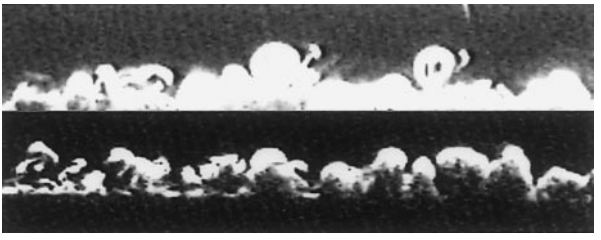

Figure 15. Representative Honji-type and quasicoherent structures at $\beta = 1\,365\,000$ and $K = 0{\cdot}10$ ($= 0{\cdot}59K_{cr}$).

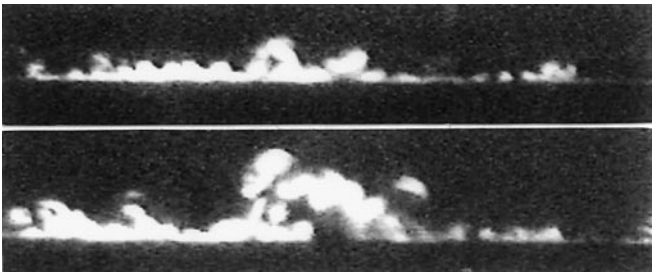

Figure 16. Representative quasicoherent structures at $\beta = 1\,365\,000$ and $K = 0{\cdot}052$ ($= 0{\cdot}31K_{cr}$).

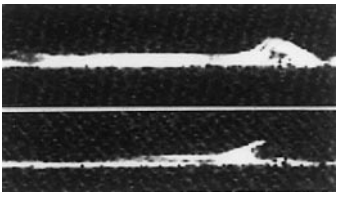

Figure 17. Representative quasicoherent structures at $\beta = 1\,365\,000$ and $K = 0{\cdot}04$ ($= 0{\cdot}24K_{cr}$).

Now, evidence of the existence of QCS in the regions first to the right and then to the left of the Hall line will be presented. Figure 13 corresponds to the point (1 365 000; 0·3) where $K \approx 1{\cdot}8\ K_{cr}$. During a given cycle the structures exhibit highly complex forms. Ejections of the fluid from the boundary are quite clear, and the structures resemble more the QCS observed in oscillatory flow on plane boundaries [see, e.g., Sarpkaya (1993)]. Figure 14 shows several examples of the behavior of flow at (120 000; 0·42) where $K = 1{\cdot}36\ K_{cr}$. It appears that at lower β values the HTCS persist even at $K > K_{cr}$ but, eventually, they too transform into QCS if K is sufficiently increased. Larger increases in K lead to increased turbulence, separation and vortex shedding and will not be discussed herein further.

Representative structures in the region where $K < K_{cr}$ will now be presented. Figure 15 shows structures at (1 365 00; 0·1) that appear to be a combination of QCS and occasional HTCS. These structures have continuously evolved during the many cycles of oscillations. Figure 16 shows at (1 365 00; 0·052) the structures that barely survive the low velocity period. In fact, with further decrease of K or β, an occasional burst occurs during the high velocity period and disappears during the low velocity period as shown in Figure 17 for (1 365 00; 0·04). Figures 18 and 19 at (300 000; 0·10) and (260 000; 0·065) show, respectively,

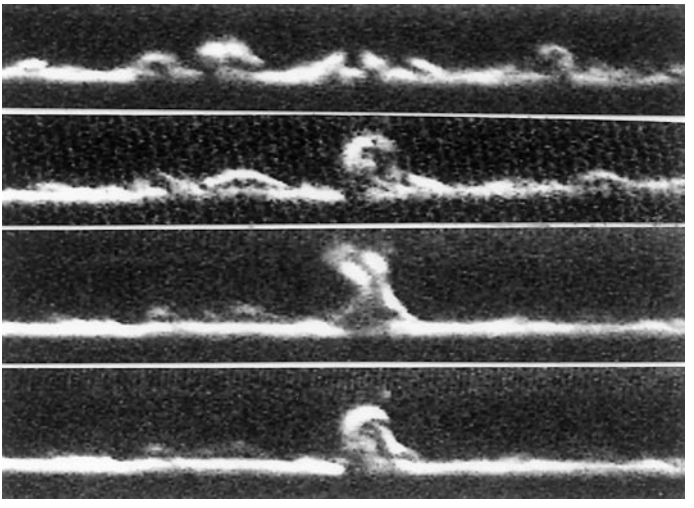

Figure 18. Representative quasicoherent structures that barely survive the acceleration period; $\beta = 300\,000$ and $K = 0{\cdot}10$ ($= 0{\cdot}4K_{cr}$).

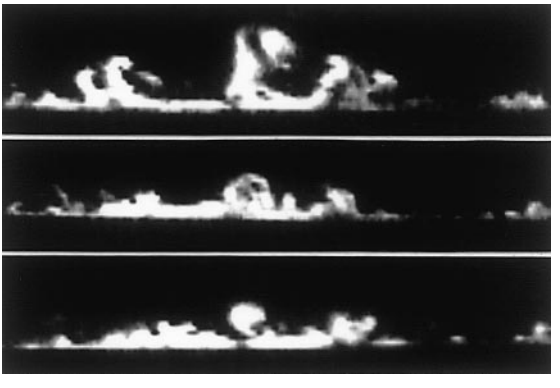

Figure 19. Representative quasicoherent structures that appear only during the deceleration period; $\beta = 260\,000$ and $K = 0{\cdot}065$ ($= 0{\cdot}25K_{cr}$).

structures that barely survive the low velocity period and those that appear only during the high velocity period. Figure 20 shows at (147 000; 0·20) the type of QCS that are very similar to those obtained in oscillatory boundary layers. At (50 000; 0·2), the QCS reduce to those shown in Figure 21 and then disappear as β is reduced to about 20 000. Figures 22 and 23 at (72 000; 0·24), and at (45 000; 0·24), respectively, show additional examples of QCS.

4.4. Quantification of the Stability Line

Previous studies of the QCS (Sarpkaya 1993) in oscillatory boundary layers have shown that the transition to turbulence in oscillatory Stokes flow is a gradual quasi-deterministic process. It has a beginning (when it is large enough to be seen), a reasonably clear intermediate step (when it exhibits a dramatic change in one or more measurable parameters), and no discernible end. For Re_δ ($\sim 2{\cdot}82\ U_{max}\delta/\nu$) ≈ 1100, one or more unevenly spaced low-speed streaks emerge toward the end of the high velocity phase and then

Figure 20. Representative quasicoherent structures that are very similar to those found in oscillatory plane boundary layers; $\beta = 147\,000$ and $K = 0{\cdot}20$ ($= 0{\cdot}68K_{cr}$).

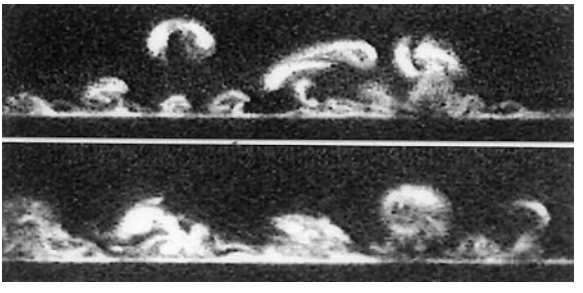

Figure 21. Smaller and weaker quasicoherent structures at $\beta = 50\,000$ and $K = 0{\cdot}20$ ($= 0{\cdot}52K_{cr}$).

completely disappear during the low velocity phase, without ever giving rise to any coherent structures. In the range of $Re_\delta \approx 1100$–1300 the vortical structures begin to emerge and continue to increase in number, over larger time intervals. The next major change occurs in the narrow interval of Re_δ values from about 2200 to 2500 in which the phase angle (the phase lead of the maximum shear stress over the maximum velocity) decreases sharply from about 34° to about 13° and the friction coefficient increases rapidly and reaches a local maximum at about $Re_\delta \approx 2800$. At these Reynolds numbers, turbulence is essentially the vestiges of more energetic structures which come into existence by violent bursting during the high velocity phase, as evidenced by extensive viewing of videotapes.

For the circular cylinder, from equation (8) and $Re = K\beta$, one has

$$Re_\delta = 2{\cdot}82\,Re\,\beta^{-1/2} = 2{\cdot}82\,K\,\beta^{1/2}. \tag{10}$$

Thus, it is natural to assume that there is a critical value of Re_δ and that equation (10) may be expressed as $K\beta^{1/2} = C$, where the constant C is to be determined from the experiments. If the Re_δ values for the flat plate and circular cylinder cases were identical, one would expect a C value of about 200 for the inception of coherent structures near the crown of the cylinder. The comparison of $K\beta^{1/2} = 200$ with the data has shown that C is too large and that the functional relationship is not in conformity with the slope of the stability line shown in Figure 7. This was not entirely unexpected on several grounds. In the plate flow, the

instability is not affected by the surface curvature or the centrifugal instability. In the case of the cylinder, it is the Taylor–Görtler instability that leads to the Hall line. In fact, as a first-order approximation to equation (4), $K\beta^{1/4} = 5{\cdot}78$ represents the fact that an instability of centrifugal type can occur when the Taylor number ($T = A^2/D\delta_{St}/K\beta^{1/4}$) exceeds a certain threshold, as noted by Hara & Mei (1990*a*). Thus, we expect that in the regions in either side of the Hall line the stability of the flow will continue to be affected by the surface curvature while undergoing instabilities of the boundary-layer type. The equation that best represents the S line is given by

$$K\beta^{2/5} = 12{\cdot}5, \tag{11}$$

which reflects the strong influence of the boundary-layer type instabilities and to a lesser extent that of the Taylor instability. Also, it is interesting to note that in a $K\beta^{2/n}$ type relationship, $n = 4$ for the flat plate, $n = 5$ for the circular cylinders, and $n = 8$ for the Honji-type instability. The Reynolds number along the stability line increases as $Re = 12{\cdot}5\beta^{3/5}$, while for $\beta = 200$, $Re = 300$; and $\beta = 10^6$, Re rises to about 50 000.

It was hoped that the instabilities will manifest themselves at K values as small as 0·0005 and β values as large as or larger than 10^6. The fact that this did not turn out to be the case was rather disappointing. It was noted earlier that the appearance of coherent structures in oscillatory flow over plane walls leads to an almost sudden and substantial increase in the skin-friction coefficient [Sarpkaya (1993) and the data shown in the references cited therein]. Should this have been the case for the K and β values shown in Figures 1 and 2, it would have provided some justification for the measured increase (almost doubling) of the drag coefficient relative to that predicted by the Stokes–Wang analysis. The use of equation (11) shows that only for K larger than about 0·044 (for $\beta = 1\,365\,000$) and 0.056 (for $\beta = 748\,000$) one should expect a significant increase in the drag coefficient and that for smaller K values the experiments should follow the Stokes–Wang line. This simply is not the case and the reasons are perplexing. One may assume that (a) there are other instabilities in other regions of the cylinder (note that we have looked only at the crown of the cylinder), (b) the instabilities become observable only when they reach a certain amplitude, not at the beginning of the laminar instability, (c) the nonlinear interactions of various types of perturbations may significantly alter the characteristics of the Stokes layer so as to increase the shear and hence the drag coefficient, and (d) the direct measurement of the drag coefficient at very low K values may simply not be reliable or sufficiently accurate. This is in spite of the fact that independent measurements (see Table 1, last entries) tend to agree with each other. It appears that it would be very desirable to simulate the rates of growth and propagation of unstable laminar wave packets on curved surfaces in reversing as well as nonreversing oscillatory boundary layers.

4.5. Flow Structures on Rough Cylinders

The profound effect of roughness on the drag and inertia coefficients of circular cylinders in sinusoidally oscillating flow has been known for about 25 years (Sarpkaya, 1976, 1977, 1978, 1987, 1990*a*,*b*). However, its relation to the Honji instability, particularly at high β values has not been explored. Experiments at smaller β values are cited in Table 1. The present experiments with two large cylinders ($k/D = 1/100$) have shown that flow separates from the sand grains at all K and β values (Figure 24). No stable region was found in the range of β values from about 10^4 to $1{\cdot}3 \times 10^6$ and K values from 0·0052 to 0·60. This does not preclude the possibility of a stable region at lower K values.

As to the Honji instability, Figure 25, corresponding to (1 365 000; 0·169), showed mushroom-like structures but they were more like real mushrooms (axisymmetric) rather

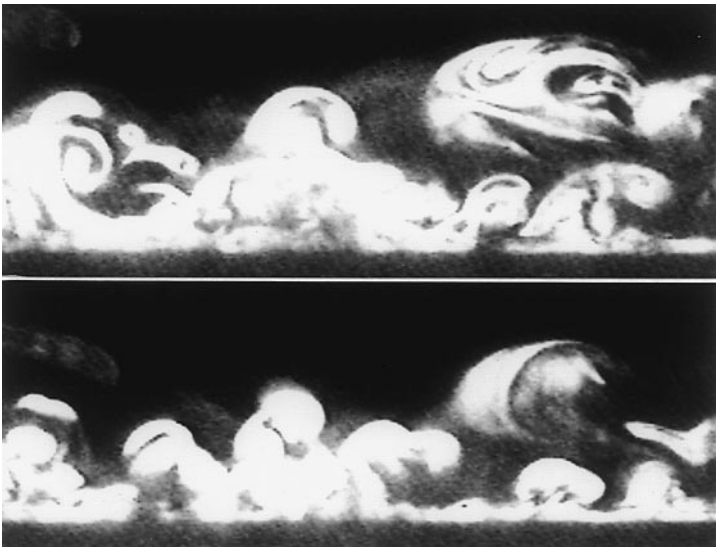

Figure 22. Additional examples of quasicoherent structures at $\beta = 72\,000$ and $K = 0{\cdot}24$ $(= 0{\cdot}68K_{cr})$.

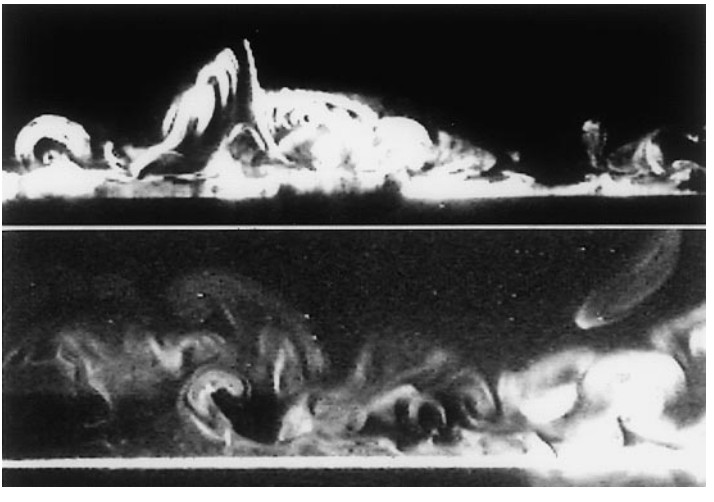

Figure 23. Additional examples of quasicoherent structures at $\beta = 45\,000$ and $K = 0{\cdot}24$ $(= 0{\cdot}60K_{cr})$.

doi:10.1006/jfls.2001.0384

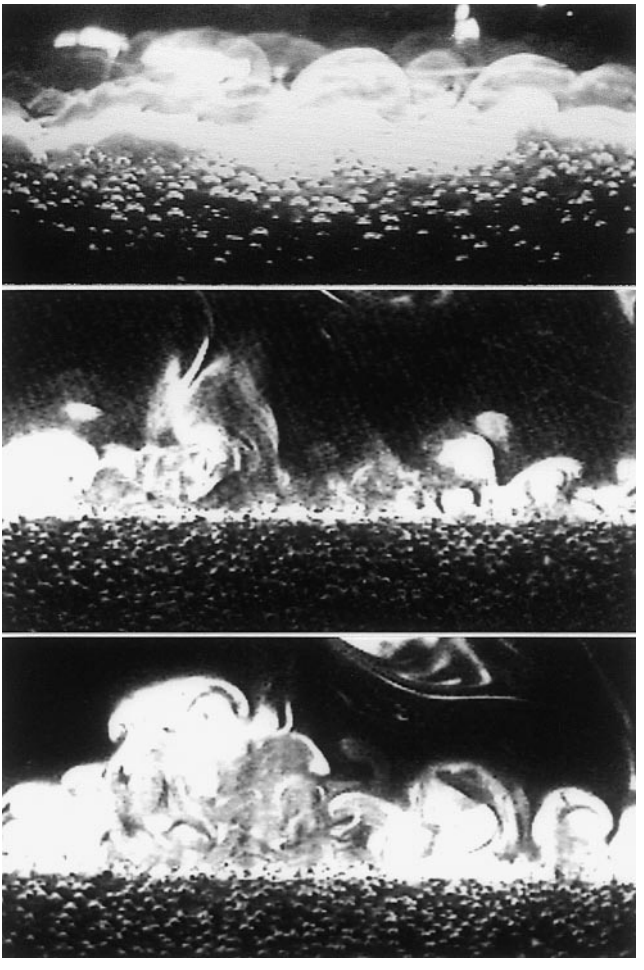

Figure 25. Representative Honji-type or quasicoherent structures on a roughened cylinder; $\beta = 1\,365\,000$ and $K = 0{\cdot}169$ (on the Hall-line).

doi:10.1006/jfls.2001.0384

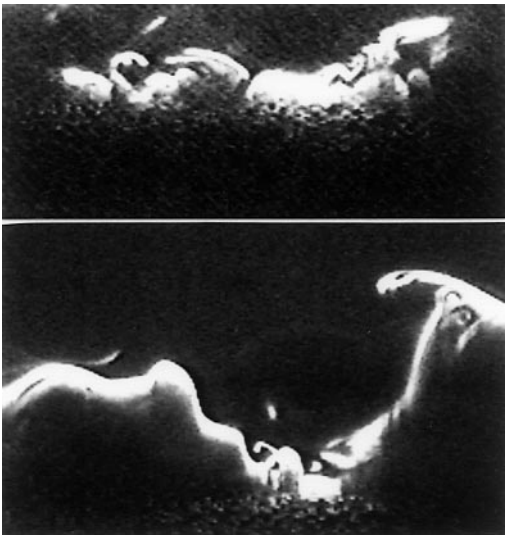

Figure 24. Close-up view of the flow separation from roughness elements on a sand-roughened cylinder.

than two-dimensional (meaning like their cross-section in a radial plane through the crown of the cylinder). They were continuously agitated as if they were boiling. The motion was often violent and the dye erupted into great heights (relative to the sand/gravel particles). There was no Honji instability in the usual sense either at this β, K point or at any other point on or off the line H. Figure 26 shows the variation of the near-wall structures during a single cycle at (147 000; 0·20). Figures 20 and 26 may be compared since they are obtained at the same β, K. These observations confirm the long-known fact that the energy dissipation on rough surfaces will be considerably larger than that for the smooth surfaces. This fact is particularly accentuated in oscillatory flow about cylinders. It remains to be seen as to how small k/D should be in order for the effect of roughness to be negligible at large β and very small K values.

4.6. Comments on Previous Experiments

In the light of the above, brief comments will be made regarding the previous work. Sarpkaya (1986), using a smoothly oscillating sinusoidal flow about a polished cylinder, found that the onset of the Honji instability spans over the interval K = 0·6–0·82 for $\beta = 1035$. This is close to $K_s = 0{\cdot}78$ at $\beta = 1035$, where K_s is the value of K on S line for a given β. Similarly, for $\beta = 1380$, ($K_s = 0{\cdot}69$), experiments exhibited a region of hysteresis as K was increased in small steps from 0·4 to about 1. Surprisingly enough, $K_s = 0{\cdot}69$ corresponds to the maximum of the first rise in C_d above the Stokes–Wang line [see Figure 2 in Sarpkaya (1986)]. Furthermore, the nature of the instability due to its sensitivity to disturbances is such that the occurrence of a region of hysteresis is not entirely unexpected. As another example of the previous work, Bearman & Russell (1996), experimenting with pluck-type decaying oscillations of smooth cylinders [see Table 1(c)] with $\beta = 16\,538$ ($K_s = 0{\cdot}26$), $\beta = 20\,526$ ($K_s = 0{\cdot}24$), $\beta = 34\,946$ ($K_s = 0{\cdot}19$), and $\beta = 61\,022$ ($K_s = 0{\cdot}15$) found that the C_d data exhibited some scatter for K values between 0·1 (their lowest K value) and about 0·25, 0·30, 0·22, and 0·15, respectively. The comparison of these

approximate K values with the corresponding K_s values suggests that the data (obtained with a cylinder subjected to pluck tests) in the region to the left of the S-line might exhibit some scatter, with some data points falling closer to the Stokes–Wang line. Otter (1990) concluded that for $\beta = 61\,400$ ($K_s = 0{\cdot}15$), damping forces agree quite well with Stokes' solution for $K < 1{\cdot}88$. This seems to be rather surprising because the flow should have been unstable for $K > 0{\cdot}15$, according to our present results, and should have been subjected to Honji instability near $K_{cr} = 0{\cdot}39$, according to Hall's analysis. The complex question of the differences between the stability lines of forced oscillation tests (at a constant amplitude and frequency) and pluck tests (with decaying amplitudes at nearly constant frequencies) is of considerable practical importance, but will not be discussed here further.

5. CONCLUDING REMARKS

An effort was made to measure the drag of circular cylinders (smooth, rough, perforated) subjected to sinusoidally oscillating motion, particularly at large values of β, to gain some insight into the magnitude of their damping and, in particular, into the reasons for the deviation of the measured values from the Stokes–Wang stable laminar flow solution. The second and probably the most important part of this effort yielded results significantly different from expectations. For smooth cylinders, the results have shown that there is a stable region in which no discernible flow structures exist near the crown of the cylinder. Then there is an unstable region where many forms of quasicoherent structures occur (for β larger than about 100). On the Hall line, these structures take the form of Honji instability even at the highest β encountered in these experiments. To the right of the Hall line, instability takes many forms and, with increasing K, falls under the influence of separation and all of its attendant consequences. Beyond a second threshold the flow becomes turbulent.

The existence of a region between the stability line S and the Hall line H can only partly explain the measured increase in the drag coefficient relative to the Stokes–Wang analysis. However, there remains a large range of K values (say between 0·0003 and the stability line) in which there is no observable instability. Even though this does not preclude the existence of evolving instabilities, it is hard to imagine that they would be large enough to nearly double the drag coefficient. Obviously, there is a need to answer this question and it will require some ingenious and difficult experiments. The use of direct numerical simulation at β values of interest here is not yet feasible. However, the tracking and quantification of similar coherent and quasicoherent structures in experimental and simulated flows, *at any point* in the K–β plane, through the use of, for example, the discriminant of the characteristic equation of the velocity gradient tensor, might help to understand not only the relationships between damping, roughness, and porosity, but also the evolution of turbulence itself.

ACKNOWLEDGEMENTS

The financial support provided by the National Science Foundation, Office of Naval Research, and the Naval Postgraduate School is gratefully acknowledged. Special thanks are due to Messrs D. B. Osgood, H. Markle, and P. Parker for their assistance in numerous ingenious ways.

REFERENCES

BEARMAN, P. W. & MACKWOOD, P. R. 1992 Measurements of the hydrodynamic damping of oscillating cylinders. In *Proceedings of the 6th International Conference on the Behavior of Offshore Structures* (BOSS '92), London, pp. 405–414.

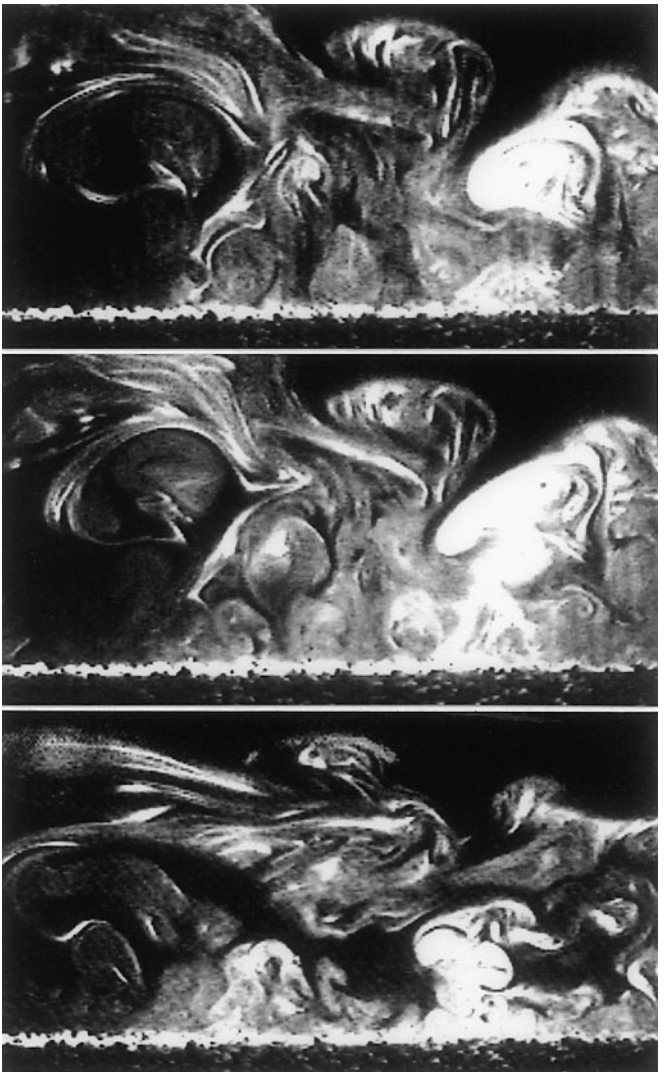

Figure 26. Representative examples of the variation of the near-wall structures on a roughened cylinder during a given cycle: $\beta = 147\,000$ and $K = 0{\cdot}2$ (see also Figure 20 at the same β–K for a smooth cylinder).

doi:10.1006/jfls.2001.0384

BEARMAN, P. W. & RUSSELL, M. P. 1996 Measurements of the hydrodynamic damping of bluff bodies with application to the prediction of viscous damping of TLP hulls. In *Proceedings of the 21st Symposium on Naval Hydrodynamics*, pp. 622–634. Washington, D. C., U.S.A.: National Academy Press.

CHAPLIN, J. R. 2000 Hydrodynamic damping of a cylinder at $\beta \approx 10^6$. *Journal of Fluids and Structures* **14,** 1101–1117.

CHAPLIN, J. R. & SUBBIAH, K. 1998 Hydrodynamic damping of a cylinder in still water and in a transverse current. *Applied Ocean Research* **20,** 251–259.

HALL, P. 1984 On the stability of unsteady boundary layer on a cylinder oscillating transversely in a viscous fluid. *Journal of Fluid Mechanics* **146,** 337–367.

HARA, T. and MEI, C. C. 1990*a* Oscillating flow over periodic ripples. *Journal of Fluid Mechanics* **211,** 183–209.

HARA, T. & MEI, C. C. 1990*b* Centrifugal instability of an oscillatory flow periodic ripples. *Journal of Fluid Mechanics* **217,** 1–32.

HONJI, H. 1981 Streaked flow around on oscillating circular cylinder. *Journal of Fluid Mechanics* **107,** 507–520.

HOWE, M. S. 1979 On the added mass of a perforated shell, with application to the generation of aerodynamic sound by a perforated trailing edge. *Proceedings of Royal Society of London*, *Series A* **365,** 209–233.

MOLIN, B. 1992 Motion damping of slotted structures. In *Hydrodynamics*: *Computations*, *Model Tests and Reality* (ed. H. J. J. van den Boom), pp. 297–303. Amsterdam: Elsevier Science Publishers.

OTTER, A. 1990 Damping forces on a cylinder oscillating in a viscous fluid. *Applied Ocean Research* **12,** 153–155.

ROBINSON, S. K. 1991 Coherent motions in the turbulent boundary layer. *Annual Review of Fluid Mechanics* **23,** 601–639. [See also, NASA Tech. Mem. 103859, 1991 and *Journal of Fluid Mechanics* **412,** 355–378].

ROBINSON, S. K. & KLINE, S. J. 1990 Turbulent boundary layer structure: progress, status and challenges. In *Structure of Turbulence and Drag Reduction* (ed. A. Gyr), pp. 3–32. Berlin: Springer-Verlag.

SARPKAYA, T. 1976 Vortex shedding and resistance in harmonic Flow about smooth and rough circular cylinders. In *Proceedings of the 1st International Conference on the Behavior of Offshore Structures* (BOSS '76), Vol. 1, pp. 220–235, The Norwegian Institute of Technology.

SARPKAYA, T. 1977 In-line and transverse forces on cylinders in oscillatory flow at high Reynolds numbers. *Journal of Ship Research* **21,** 200–216.

SARPKAYA, T. 1978 Hydrodynamic resistance of roughened cylinders in harmonic flow. *Journal of the Royal Institute of Naval Architects* **120,** 41–55.

SARPKAYA, T. 1986 Force on circular cylinder in viscous oscillatory flow at low Keulegan–Carpenter numbers. *Journal of Fluid Mechanics* **165,** 61–71.

SARPKAYA, T. 1987 Oscillating flow about smooth and rough cylinders. *ASME Journal of Offshore Mechanics and Arctic Engineering* **109,** 113–121.

SARPKAYA, T. 1990*a* Wave forces on cylindrical piles. In *The Sea*, *Ocean Engineering Science* (eds B. Le Mehaute & D. M. Haynes), pp. 169–195. New York: John Wiley & Sons.

SARPKAYA, T. 1990b On the effect of roughness on cylinders. *ASME Journal of Offshore Mechanics and Arctic Engineering* **112,** 334–340.

SARPKAYA, T. 1993 Coherent structures in oscillatory boundary layers. *Journal of Fluid Mechanics* **253,** 105–140.

SARPKAYA, T. 2000 Time-dependent flow about solid and perforated cylinders. Paper presented at the *IUTAM Symposium on Bluff Body Wakes and Vortex-Induced Vibrations*, 13–16 June 2000, Marseille, France.

SMITH, C. R., WALKER, J. D. A., HAIDARI, A. H. & SOBRUN, U. 1991 On the dynamics of near-wall turbulence. *Philosophical Transactions Royal Society London* **A-336,** 131–175.

SCANDURA, P., VITTORI, G. & BLONDEAUX, P. 2000 Three-dimensional oscillatory flow over steep ripples. *Journal of Fluid Mechanics* **412,** 355–378.

STOKES, G. G. 1851 On the effect of the internal friction of fluids on the motion of pendulums. *Transactions of the Cambridge Philosophical Society* **9,** 8–106.

TROESCH, A. W. & KIM, S. K. 1991 Hydrodynamic forces acting on cylinders oscillating at small amplitudes. *Journal of Fluids and Structures* **5,** 113–126.

WANG, C.-Y. 1968 On the high frequency oscillating viscous flows. *Journal of Fluid Mechanics* **32,** 55–68.

ZHANG, J. & DALTON, C. 1999 The onset of three-dimensionality in an oscillating flow past a fixed circular cylinder. *International Journal for Numerical Methods in Fluids* **30,** 19–42.